V European Conference on Computational Fluid Dynamics
ECCOMAS CFD 2010
J. C. F. Pereira and A. Sequeira (Eds)
Lisbon, Portugal,14-17 June 2010

A 2D COMPACT FINITE DIFFERENCE IMMERSED BOUNDARY METHOD FOR FLOW IN POROUS MEDIA

Paulo J. S. A. Ferreira de Sousa[*,†] **and Isabel Malico**[†,††]

[*]Vanderbilt University,
Department of Mechanical Engineering, Nashville, TN, USA
e-mail: ferreiradesousa@gmail.com
[†]IDMEC/IST,Technical University of Lisbon,
Mechanical Engineering Department, Av. Rovisco Pais, 1049-001 Lisbon, Portugal
[††]University of Évora,
Physics Department, R. Romão Ramalho, 59, 7000-671 Évora, Portugal
e-mail: imbm@uevora.pt

Key words: Immersed Boundary Method, Incompressible Navier–Stokes, Compact Finite Differences, Square Obstacles, Porous Media

Abstract. *We present a compact finite differences method for the calculation of two-dimensional viscous flows in porous media. This is achieved by using body forces that allow for the imposition of boundary conditions that coincide with the computational grid. An implementation of the forcing of Mohd-Yusof[1] is used in order to implement the immersed boundary. A detailed description of the original compact finite difference method used can be found in Ferreira de Sousa et al.[2] The unsteady, incompressible Navier-Stokes equations are solved in a Cartesian staggered grid with fourth-order Runge-Kutta temporal discretization and fourth-order compact schemes for spatial discretization, used to achieve highly accurate calculations. Special attention is given to the boundary condition implementation on the immersed media.*

In this paper, two different flows are calculated. First, the flow over a 2D square cylinder located along the centreline of a channel with free-slip boundary conditions. The computed drag coefficient is compared with numerical results available in the literature. The second flow configuration analyzed is the flow over a porous matrix composed of staggered square cylinders. Results for the pressure drop across the porous matrix are presented for a wide range of Reynolds numbers, along with flow visualization.

1 INTRODUCTION

The study of transport phenomena in porous media is important due to the many engineering applications it possesses. If one focus on energy conversion applications only, combustion or gasification of biomass can be regarded as occurring in non-inert porous media (e.g., di Blasi[3] and van der Lans[4]); or, alternatively, inert porous media can integrate equipment that involve the recovery of what would be otherwise waste energy or that burn hydrogen, biogas or more conventional fuels (e.g., Wood and Harris[5] and Mendes et al.[6]). Non-Darcian flow is common on such technological applications and a flexible and accurate computational tool is required to predict it.

Almost all the numerical studies dedicated to flow and heat transfer in porous media rely on semi-empirical derivations of the volume-averaged forms of the transport equations - continuum approach (e.g., Howell et al.,[7] Bouma and de Goey,[8] Brenner et al.,[9] Malico and Pereira,[10] Barra and Ellzey,[11] Pereira et al.[12] and Hayashi et al.[13]). This approach is very valuable and capable of giving relatively fast answers to the macroscopic characteristics of the problems studied, but is incapable of dealing with the pore level characteristics, which are sometimes determinate to explain certain phenomena, such as, flashback in low porosity porous media and NOx formation (See for example, Sahraoui and Kaviany[14] and Hayashi et al.[13]). Moreover, when using the volume-average forms of the transport equations, closure models are needed for the equations since a large number of unknowns are introduced by the averaging procedure. These models are based either on experiments or simple geometry numerical simulations due to the complexity of the flow paths and the interpore and pore-to-pore fluid dynamic interactions (e.g., Macdonald et al.,[15] Pedras and Lemos[16] and Alshare et al.[17]).

To be able to predict pore level characteristics, a direct numerical simulation, DNS, of the flow field has to be undertaken. There are examples of such simulations (e.g., Sahraoui and Kaviany,[14] Pedras and Lemos[16] and Breugem and Boersma[18]); however, often the porous media have a relatively simple geometry, such as 2D arrays of cylinders. Also, when trying to simulate microscopically the flow and heat transfer in porous media, mainly boundary fitted grids have been used. This procedure presents two significant disadvantages: i) fitting a grid to a complex geometry prevents the use of simple orthogonal grids and ii) generating a boundary fitted grid for a complex geometry can be extremely time consuming and difficult.[19] An alternative to the boundary fitted curvilinear method and unstructured mesh technique that overcomes this advantages is the simulation of immerse boundaries on Cartesian grids. This is the path followed in this work.

Breugem and Boersma[18] were the first to apply the immersed boundary method, IBM, to enforce the no-slip and no-penetration conditions on the cubes constituting the porous media. They compared the results of DNS and the continuum approach, and found a very good agreement. Sahraoui and Kaviany[14] also compared the continuum and the volume-average approaches to simulate not only momentum, but also heat and reacting species transport with no radiation. However, they considered boundary fitted grids and

simple 2D porous media. It was demonstrated that, for the macroscopic characteristics, the volume averaged model preformed well, but could not predict pore level phenomena.

Immersed boundary methods have gained popularity for their ability to handle complex surface geometry.[19] Peskin[20,21] first introduced the method by describing the flow field with an Eulerian discretization and representing the immersed surface with a set of Lagrangian points. Methods such as those of Peskin fall in the category of methods that employ "continuous forcing". A second category consists of methods that employ discrete forcing, where the forcing is either explicitly or implicitly applied to the discretized Navier-Stokes equations. These include methods of Ye et al.,[22] Fadlun et al.,[23] Udaykumar et al.,[24] Kim et al.,[25] Ghias et al.,[26] Ferreira de Sousa et al.[2] and others. The key advantage for the methods in the second category is that for certain formulations, a sharp representation of the immersed boundary is possible.[24] In Mital et al.,[27] a finite-difference based immersed boundary method that allows simulating complex 3D flows with moving immersed boundaries is presented.

More recently, Paravento et al.[28] used an IBM to calculate a geometry consisting of a square body in a flow (not a porous medium, but what could be looked like the building block of a simple porous medium). The method is applied to flow cases with and without heat transfer. This approach has already been successfully applied by Breugem and Boersma,[18] but it was extended for the case of heat transfer between body and flow.

In this paper, a compact finite differences method is used for the calculation of two-dimensional viscous flows both over a square cylinder and in a porous matrix composed of staggered square cylinders. This is achieved by using body forces that allow for the imposition of the boundary conditions that coincide with the computational grid. An implementation of the forcing of Mohd-Yusof[1] is used in order to implement the immersed boundary. The unsteady, incompressible Navier-Stokes equations are solved in a Cartesian staggered grid with third-order Runge-Kutta temporal discretization and fourth-order compact schemes for spatial discretization, used to achieve highly accurate calculations. The results obtained for the flow over a square cylinder are obtained for validation with the data of other authors.[28,30] As far as the simulations through the porous matrix are concerned, pressure forces are shown for several Reynolds numbers, along with flow visualization.

2 GOVERNING EQUATIONS

The unsteady incompressible form of the continuity and Navier–Stokes equations for a Newtonian fluid were considered

$$\nabla \cdot \mathbf{u} = 0 \tag{1}$$

$$\frac{\partial \mathbf{u}}{\partial t} + (\mathbf{u} \cdot \nabla)\mathbf{u} = \nu \nabla^2 \mathbf{u} - \nabla p + \mathbf{f} \tag{2}$$

where $\mathbf{u}$ is the fluid velocity, p the pressure (divided by density), ν the kinematic viscosity of the fluid and $\mathbf{f}$ is a body-force field.

3 NUMERICAL SCHEMES

The momentum equations are spatially discretized on a Cartesian staggered mesh by finite differences and all derivatives are evaluated with implicit 4th-order accurate compact finite difference schemes.[31] The fourth order accurate Runge–Kutta scheme was used for temporal discretization. The numerical method used belongs to the projection methods class, and the resulting Poisson equation was also discretized with compact operators. The procedure is presented in the Ferreira de Sousa's papers.[2,32]

For the sake of simplicity, let us consider a uniformly spaced mesh where the nodes are indexed by j, as shown in Figure 1. The independent variable at the nodes is $x_j = h(j-1)$ for $1 \leq j \leq N$, where $h = x_{j+1} - x_j$, and the function values at the nodes $f_j = f(x_j)$ are given.

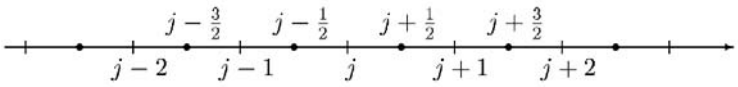

Figure 1: 1D grid for collocated and staggered schemes

3.1 Approximation of First Derivative

The finite difference approximation f'_j to the first derivative at the node j depends on the function values at nodes near j. These schemes are generalizations of the Padé scheme. These generalizations are derived by writing approximations of the form

$$\beta f'_{j-2} + \alpha f'_{j-1} + f'_j + \alpha f'_{j+1} + \beta f'_{j+2} = a\frac{f_{j+1} - f_{j-1}}{2h} + b\frac{f_{j+2} - f_{j-2}}{4h} + c\frac{f_{j+3} - f_{j-3}}{6h} \quad (3)$$

The relations between the coefficients α, β, a, b and c are derived by matching the Taylor series coefficients of various orders. For the 4th order tri-diagonal scheme (Classical Padé scheme):

$$\alpha = \frac{1}{4}, \beta = 0, a = \frac{3}{2}, b = 0, c = 0 \quad (4)$$

3.2 Approximation of Second Derivative

The derivation of compact approximations for the second derivative is similar to the first derivative. Again we start with a relation of the following form

$$\beta f''_{j-2} + \alpha f''_{j-1} + f''_j + \alpha f''_{j+1} + \beta f''_{j+2} = a\frac{f_{j+1} - 2f_j + f_{j-1}}{h^2} + b\frac{f_{j+2} - 2f_j + f_{j-2}}{4h^2} + \quad (5)$$
$$+ c\frac{f_{j+3} - 2f_j + f_{j-3}}{9h^2}$$

where f''_j represents the finite difference approximation to the second derivative at node j. Once again, the relations between the coefficients α, β, a, b and c are derived by matching the Taylor series coefficients of various orders. For the 4th order tri-diagonal scheme:

$$\alpha = \frac{1}{10}, \beta = 0, a = \frac{6}{5}, b = 0, c = 0 \tag{6}$$

3.3 Approximation of First Derivative on Cell-centered Mesh

Formulas for calculating the first derivative on a cell-centered mesh are necessary in staggered grids. Referring again to Figure 1 and starting from an approximation of the form

$$\beta f'_{j-2} + \alpha f'_{j-1} + f'_j + \alpha f'_{j+1} + \beta f'_{j+2} = a\frac{f_{j+1/2} - f_{j-1/2}}{h} + b\frac{f_{j+3/2} - f_{j-3/2}}{3h} + \\ + c\frac{f_{j+5/2} - f_{j-5/2}}{5h} \tag{7}$$

the relations between the coefficients α, β, a, b and c are derived yet again by matching the Taylor series coefficients of various orders.

For the 4th order tri-diagonal scheme:

$$\alpha = \frac{1}{22}, \beta = 0, a = \frac{12}{11}, b = 0, c = 0 \tag{8}$$

4 BOUNDARY SCHEMES

Most problems of physical interest involve domains with non-periodic boundaries. In order to handle these, boundary schemes need to be implemented for differentiation and interpolation at the boundary nodes. These schemes involve one-sided differencing and need to possess an order of accuracy as high as possible, see for example Mahesh.[33] Boundary schemes satisfying these requirements are presented in this section.

In a staggered grid, two sets of boundary schemes are required. Lets consider the 1D grid shown in Figure 2 which shows the nodes and the numbering scheme at the left boundary.

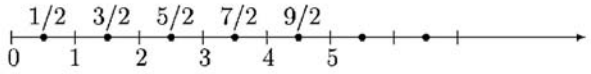

Figure 2: 1D variable arrangement at left boundary

4.1 Boundary Schemes for the First Derivative

A scheme for the first derivative at the boundary node ($j = 0$) may be written as

$$f'_0 + \hat{\alpha} f'_1 = \frac{1}{\Delta x}(a f_{1/2} + b f_{3/2} + c f_{5/2} + d f_{7/2}) \tag{9}$$

In this implementation, we used a third-order scheme given by:

$$\begin{aligned} \hat{\alpha} &= 23 \\ a &= -25 \\ b &= 26 \\ c &= -1 \end{aligned} \tag{10}$$

The first derivative at the boundary ($j = 1/2$) can be written as

$$f'_{1/2} + \hat{\alpha} f'_{3/2} = \frac{1}{\Delta x}(a f_0 + b f_1 + c f_2 + d f_3) \tag{11}$$

Again, the third-order scheme is given by:

$$\begin{aligned} \hat{\alpha} &= -1 \\ a &= -1 \\ b &= 2 \\ c &= -1 \end{aligned} \tag{12}$$

4.2 Boundary Schemes for Interpolation

A scheme for interpolating a function to the boundary ($j = 0$) can be written as

$$f_0 + \hat{\alpha} f_1 = (a f_{1/2} + b f_{3/2} + c f_{5/2}) \tag{13}$$

Matching coefficients of the Taylor expansion gives a third-order scheme with

$$\begin{aligned} a &= \frac{1}{8}(3\hat{\alpha} + 15) \\ b &= \frac{1}{4}(3\hat{\alpha} - 5) \\ c &= \frac{1}{8}(3 - \hat{\alpha}) \end{aligned} \tag{14}$$

For simplicity, the scheme with $\hat{\alpha} = 0$ was used in all calculations.
The interpolation scheme for the boundary node ($j = 1/2$) is written as

$$f_{1/2} + \hat{\alpha} f_{3/2} = a f_0 + b f_1 + c f_2 + d f_3 \tag{15}$$

This allows for a fourth-order scheme with

$$\begin{aligned} a &= \frac{1}{16}(5 - \hat{\alpha}) \\ b &= \frac{1}{16}(9\hat{\alpha} + 15) \\ c &= \frac{1}{16}(9\hat{\alpha} - 5) \\ d &= \frac{1}{16}(1 - \hat{\alpha}) \end{aligned} \tag{16}$$

where $\hat{\alpha} = 0$ once again is chosen for simplicity.

5 IMMERSED BOUNDARY

One possibility for the solution of the IB problem is to have a body-force field $\mathbf{f}$ such that a desired velocity distribution $\mathbf{V}$ can be assigned over a boundary $\mathbf{S}^1$. In other words, from the body–force $\mathbf{f}$ added to the Navier–Stokes equations we can solve for $\mathbf{u}$ explicitly. In principle there are no restrictions for the velocity distribution $\mathbf{V}$ and for the shape and motion of $\mathbf{S}$. The main advantage of this approach is that $\mathbf{f}$ can be prescribed on a regular mesh so that the accuracy and efficiency of the solution procedure on simple grids are maintained. If Equation 2 is discretized in time, we have

$$\frac{\mathbf{u}^{t+1} - \mathbf{u}^t}{\Delta t} = RHS^{t+1/2} + \mathbf{f}^{t+1/2} \tag{17}$$

where $RHS^{t+1/2}$ contains convective and viscous terms and the pressure gradient. If now we ask which value of $\mathbf{f}^{t+1/2}$ will yield $\mathbf{u}^{t+1} = \mathbf{V}^{t+1}$ on the IB the answer is simply given from the above equation,

$$\mathbf{f}^{t+1/2} = -RHS^{t+1/2} + \frac{\mathbf{V}^{t+1} - \mathbf{u}^t}{\Delta t} \tag{18}$$

This forcing is direct in the sense that the desired value of velocity is imposed directly on the boundary without any dynamical process. Therefore, at every time step, the boundary condition holds regardless of the frequencies in the flow.

5.1 Immersed Obstacle Implementation

The expressions given for the forcing are accurate if the position of the unknowns on the grid coincides with that of the IB. This is the case for the immersed obstacle implementation presented in this paper. This requires the boundary to lie on coordinate lines or surfaces. In the present case, where a staggered grid is used, the boundary is coincident with the position where velocity component is defined, i.e. a whole cell is forced when defining the shape of the obstacle (Figure 3). Mohd-Yusof's[1] and Fadlun et al.[23] original implementations were on a staggered grids too.

Since the forcing is used to enforce the velocity on the boundary, the x-direction force is calculated on the u-grid and the y-direction force is calculated on the v-grid.

The forcing procedure used is the following. For each stage of the RK-4 time discretization:

1 Forcing points are defined as the points that lie on coordinate lines corresponding to the shape of the IB.

3 Forcing velocity $\mathbf{V}^{t+1}$ is calculated directly from the Dirichlet boundary condition.

4 The body force $\mathbf{f}$ is calculated using Equation 18.

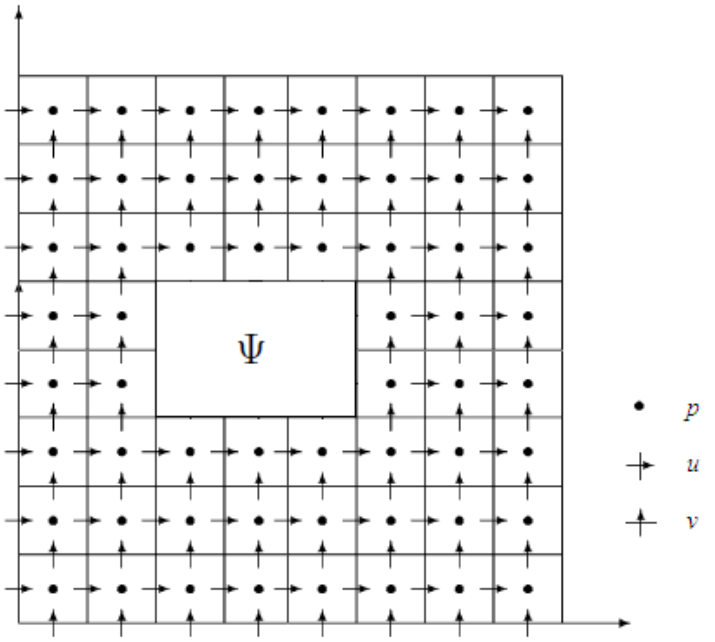

Figure 3: Immersed boundary method staggered grid arrangement

As it will be shown in the results section, the velocity boundary conditions on Ψ are satisfied "exactly" within the overall accuracy of the scheme. Pressure boundary conditions are not imposed on Ψ but they are implicit into the RHS of the Poisson equation, since the momentum equation normal do the boundary reduces to $\mathrm{d}p/\mathrm{d}n = 0$ on the boundary points[34] (see Fadlun et al.[23] for a detailed discussion).

6 RESULTS

We present the simulations of two distinct flow configurations. The first geometry was chosen with the objective of comparing our results with other authors data. It is the laminar flow over a bi-dimensional square cylinder. The second flow configuration allows showing the potential of the method, since it is a complex flow over a porous matrix composed of staggered square cylinders.

6.1 Flow over a Square Cylinder

In this section we present the bi-dimensional flow over a square cylinder placed at the centreline of a channel with free-slip boundary conditions at the walls. The cylinder has a diameter D and is placed $4.5D$ from the inlet. The length of the channel is $20D$ and its height $12D$. The inflow velocity is unity and the simulated Reynolds numbers are 100, 150, 200, 250 and 300.

Figure 4 shows the mean drag coefficient as a function of the Reynolds number for the 2D calculations of the flow over a square cylinder. The results are compared to the

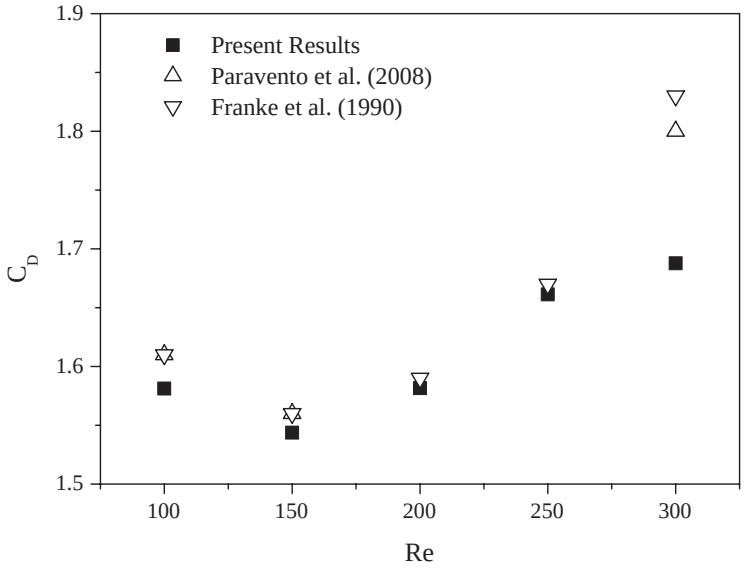

Figure 4: Mean drag coefficient versus Reynolds number for a square cylinder

numerical results of Franke et al.,[30] which were validated with experimental data, and Paravento et al.[28] The present results are in good agreement with the reference data.

6.2 Flow through a Porous Matrix

The flow through an array of staggered square cylinders was simulated for five different Reynolds numbers: 200, 500, 1000, 2000 and 5000. The implemented porous matrix geometry can be seen in Figure 5. Dirichlet boundary conditions are imposed at the walls, inlet boundary conditions at the inlet and open boundary conditions at the outlet.

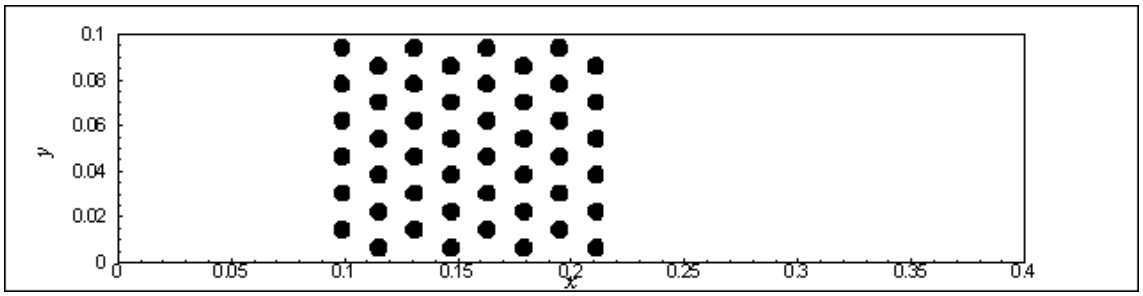

Figure 5: Staggered square cylinders matrix implemented

Figure 6 shows the pressure force as a function of the Reynolds number for $t = 10s$. For higher Reynolds numbers, the pressure force is lower, since the viscosity is lower.

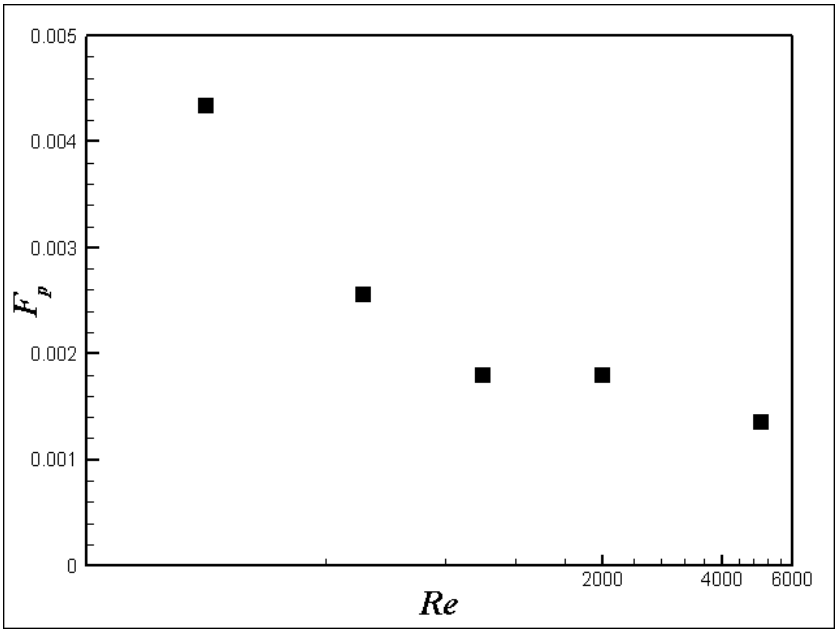

Figure 6: Pressure force versus Reynolds number for the flow through an array of staggered square cylinders ($t = 10s$)

Figures 7 (a)-(e) show the vorticity fields for the computed Reynolds numbers at $t = 10s$. For the lower Reynolds numbers simulated, the wakes of the cylinders seem to be almost unperturbed by the other cylinders. As the Reynolds number increases, so does the length of the wakes and, at a Reynolds number of 2000, vortices like the ones observed in the Karman vortex street develop and merge. It can be seen that for the higher Reynolds numbers, the wakes of the upstream cylinders are reduced and stabilized by the presence of the downstream obstacles.

7 CONCLUSIONS

A bi-dimensional compact finite difference immersed boundary method is used to simulate two different flow configurations. The flow over a square cylinder was chosen to compare the present results with the data from other authors. The mean drag coefficients for different Reynolds numbers in the range of 100 to 300 are compared with the data of Franke et al.[30] and Paravento et al.[28] The agreement between the different results is good.

The simulation of the flow through a complex geometry (staggered arrangement of square cylinders) highlights the potential of immersed boundary methods. Visualization of the vorticity field for five Reynolds numbers ranging from 200 to 5000 and the pressure force versus the Reynolds number are shown.

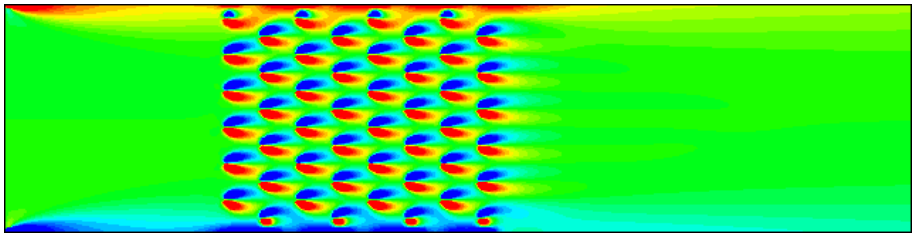

(a) Re=200

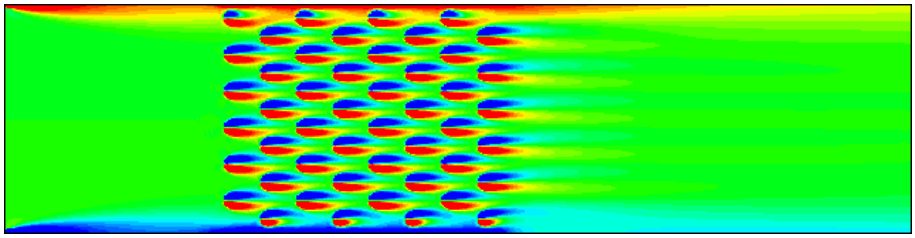

(b) Re=500

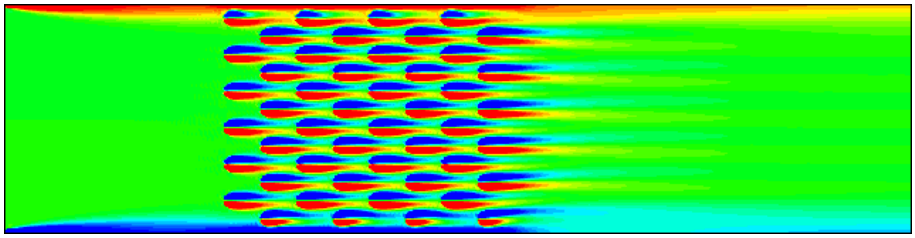

(c) Re=1000

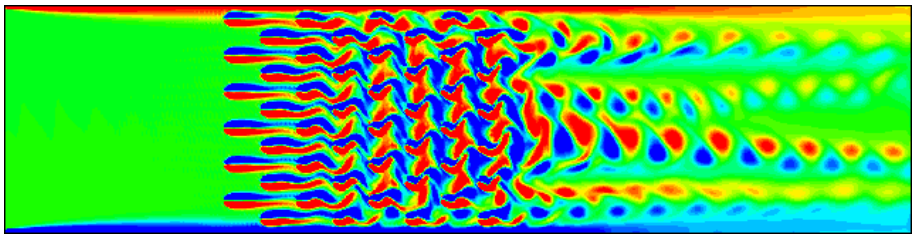

(d) Re=2000

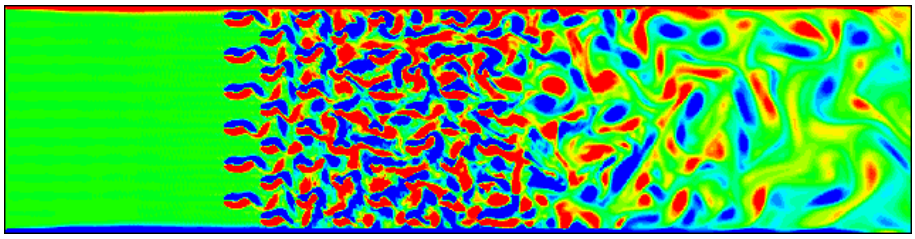

(e) Re=5000

Figure 7: The vorticity field for several Reynolds numbers.

8 ACKNOWLEDGEMENTS

The authors would like to thank FCT – *Fundação para a Ciência e a Tecnologia*, for the funding under the project PTDC/EME-MFE/100178/2008. Additionally Paulo Ferreira de Sousa would like to acknowledge the grant by FCT (SFRH/BPD/48160/2008).

REFERENCES

[1] J. Mohd-Yusof, Combined Immersed Boundaries/B–Splines Methods for Simulations of Flows in Complex Geometries, *CTR Annual Research Briefs* (1997).

[2] P. J. S. A. Ferreira de Sousa, J. C. F. Pereira and J. J. Allen, Two-dimensional compact finite difference immersed boundary method, *Int. J. Numer. Meth. Fluids*, accepted for publication (2009).

[3] C. di Blasi, Dynamic behaviour of stratified downdraft gasifiers, *Chemical Engineering Science*, **55**, 2931–2944 (2000).

[4] R. P. van der Lans, L. T. Pedersen, A. Jensen, P. Glarborg and K. Dam-Johansen, Modelling and experiments of straw combustion in a grate furnace, *Biomass and Bioenergy*, **19**, 199–208 (2000).

[5] S. Wood and A. T. Harris, Porous burners for lean-burn applications, *Progress in Energy and Combustion Science*, **34**, 667–684 (2008).

[6] M. A. A. Mendes, J. M. C. Pereira and J. C. F. Pereira, On the stability of ultra-lean H2/CO combustion in inert porous burners, *International Journal of Hydrogen Energy*, **33**, 3415–3425 (2008).

[7] J. R. Howell, M. J. Hall and J. L. Ellzey, Combustion of hydrocarbon fuels within porous inert media, *Progress in Energy and Combustion Science*, **22**, 121–145 (1996).

[8] P. H. Bouma and L. P. H. de Goey, Premixed combustion on ceramic foam burners, *Combustion and Flame*, **119**, 133–143 (1996).

[9] G. Brenner, K. Pickenäcker, O. Pickenäcker, D. Trimis, K. Wawrzinek and T. Weber, Numerical and experimental investigation of matrix-stabilized methane/air combustion in porous inert media, *Combustion and Flame*, **123**, 201–213 (2000).

[10] I. Malico and J. C. F. Pereira, Numerical study on the influence of radiative properties in porous media combustion, *ASME Journal of Heat Transfer*, **123**, 951–957 (2001).

[11] A. J. Barra and J. L. Ellzey, Heat recirculation and heat transfer in porous burners, *Combustion and Flame*, **137**, 230–241 (2004).

[12] J. C. F. Pereira, I. Malico, T. C. Hayashi and J. M. F. Raposo, Experimental and numerical characterization of the transverse dispersion at the exit of a short ceramic foam inside a pipe, *International Journal of Heat and Mass Transfer*, **48**, 1–14 (2005).

[13] T. C. Hayashi, I. Malico and J. C. F. Pereira, Influence of the preheating layer characteristics in a two-layer porous burner, *CLEAN AIR: International Journal on Energy for a Clean Environment*, **8**, 125–143 (2007).

[14] M. Sahraoui and M. Kaviany, Direct simulation vs. volume-averaged treatment of adiabatic, premixed flame in a porous medium, *International Journal of Heat and Mass Transfer*, **37**, 2817–2834 (1994).

[15] I. F. Macdonald, M. S. El-Sayed, K. Mow and F. A. L. Dullien, Flow through porous media - Ergun equation revisited, *Industrial and Engineering Chemistry Fundamentals*, **18**, 199–208 (1979).

[16] M. H. J. Pedras and M. J. S. de Lemos, Macroscopic turbulence modeling for incompressible flow through undeformable porous media, *International Journal of Heat and Mass Transfer*, **44**, 1081–1093 (2001).

[17] A. A. Alshare, P. J. Strykowski and T. W. Simon, Modeling of unsteady and steady fluid flow, heat tranfer and dispersion in porous media using unit cell scale, *International Journal of Energy and Mass Transfer*, **53**, 2294–2310 (2010).

[18] W. P. Breugem and B. J. Boersma, Direct numerical simulations of turbulent flow over a permeable wall using a direct and a continuum approach, *Physics of Fluids*, **17**, 025103 (2005).

[19] R. Mittal and G. Iaccarino, Immersed boundary methods, *Ann. Rev. Fluid Mech.*, **37**, 39–261 (2005).

[20] C. S. Peskin, Flow patterns around heart valves: a numerical method, *J. Comput. Phys.*, **10**, 252–271 (1972).

[21] C. S. Peskin, The immersed boundary method, *Acta Numerica*, **11**, 479–517 (2002).

[22] T. Ye, R. Mittal, H. S. Udaykumar and W. Shyy, An accurate Cartesian grid method for viscous incompressible flows with complex immersed boundaries, *J. Comput. Phys.*, **156**, 209–240 (1999).

[23] E. A. Fadlun, R. Verzicco, P. Orlandi and J. Mohd-Yusof, Combined immersed boundary finite-difference methods for three-dimensional complex flow simulations, *J. Comput. Phys.*, **161**, 35–60 (2000).

[24] H. S. Udaykumar, R. Mittal, P. Rampunggoon and A. Khanna, A sharp interface cartesian grid method for simulating flows with complex moving boundaries, *J. Comput. Phys.*, **174**, 345–380 (2001).

[25] J. Kim, D. Kim and H. Choi, An immersed-boundary finite-volume method for simulations of flow in complex geometries, *Journal of Computational Physics*, **171**, 132–150 (2001).

[26] R. Ghias, R. Mittal, and H. Dong, A sharp interface immersed boundary method for compressible viscous flows, *J. Comput. Phys.*, **225**, 528–553 (2007).

[27] R. Mittal, H. Dong, M. Bozkurttas, F. M. Najjar, A. Vargas and A. vonLoebbeck, A versatile sharp interface immersed boundary method for incompressible flows with complex boundaries, *J. Comput. Phys.*, **227**, 4825–4852 (2008).

[28] F. Paravento, M. J. Pourquie and B. J. Boersma, An immersed boundary method for complex flow and heat transfer, *Flow Turbulence Combust.*, **80**, 187–206 (2008).

[29] J. R. Pacheco, A. Pacheco-Vega, T. Rodi and R. E. Peck, Numerical simulations of heat transfer and fluid flow problems using an immersed-boundary finite-volume method on nonstaggered grids, *Numerical Heat Transfer, Part B: Fundamentals*, **48**, 1–24 (2005).

[30] R. Franke, W. Rodi and B. Schönung, Numerical calculations of laminar vortex-shedding flow past cylinders, *J. Wind Eng. Ind. Aerodyn.*, **35**, 237–257 (1990).

[31] S. K. Lele, Compact finite difference schemes with spectral-like resolution, *J. Comput. Phys.*, **103**, 16–42 (1992).

[32] P. J. S. A. Ferreira de Sousa and J. C. F. Pereira, Fourth– and tenth–order compact finite difference solutions of perturbed circular vortex flows, *Int. J. Numer. Meth. Fluids* , **49**, 603–618 (2005).

[33] K. Mahesh, A family of high order finite difference schemes with good spectral resolution, *J. Comput. Phys.*, **145**, 332–358 (1998).

[34] E. Balaras, Modeling complex boundaries using an external force field on fixed Cartesian grids in large-eddy simulations, *Computers & Fluids.*, **33**, 375–404 (2004).